Published in final edited form as:
Dev Cell. 2008 May ; 14(5): 775–786. doi:10.1016/j.devcel.2008.02.014.

Local actin-dependent endocytosis is zygotically controlled to initiate Drosophila cellularization

Anna Marie Sokac[1] and **Eric Wieschaus**[1,2]

[1]Department of Molecular Biology, Princeton University

[2]Howard Hughes Medical Institute, Princeton University

Summary

In early Drosophila embryos, several mitotic cycles proceed with aborted cytokinesis before a modified cytokinesis, called cellularization, finally divides the syncytium into individual cells. Here we find that scission of endocytic vesicles from the plasma membrane (PM) provides a control point to regulate the furrowing events that accompany this development. At early mitotic cycles, local furrow-associated endocytosis is controlled by cell cycle progression, whereas at cellularization, which occurs in a prolonged interphase, it is controlled by expression of the zygotic gene *nullo*. *nullo* mutations impair cortical F-actin accumulation and scission of endocytic vesicles, such that membrane tubules remain tethered to the PM and deplete structural components from the furrows, precipitating furrow regression. Thus, Nullo regulates scission to restrain endocytosis of proteins essential for furrow stabilization at the onset of cellularization. We propose that developmentally regulated endocytosis can coordinate actin/PM remodeling to directly drive furrow dynamics during morphogenesis.

Introduction

Morphogenesis is the product of a developmental program that controls complex cellular mechanisms to shape cells, tissues and whole organisms. Endocytosis represents one cellular mechanism that is tightly controlled during morphogenesis to change the position and trafficking of morphogens, signaling receptors, polarity cues and adhesion molecules (Dudu et al., 2004; Emery and Knoblich, 2006), and so influences cell fate and proliferation within cell populations. But endocytosis is equally well-suited to coordinate the timely remodeling of the PM and cytoskeleton at specific sites within single cells. Endocytosis adjusts cell surface area in both dividing and crawling cells (Boucrot and Kirchhausen, 2007; Traynor and Kay, 2007), and asymmetrically distributes proteins within the cortex of polarized cells (Marco et al., 2007; Men et al., 2008). Moreover, components of the endocytic machinery are shared with the actin cytoskeleton (Smythe and Ayscough, 2006), suggesting that endocytosis couples actin and membrane dynamics. Thus, endocytosis emerges as a possible target for developmental control that could coordinate PM and actin remodeling to directly drive cell shape change during morphogenesis.

Contact: Eric Wieschaus, Washington Road, Princeton, NJ 08544, USA, efw@princeton.edu, Phone: (609) 258-5383, Fax: (609) 258-1547.

During early morphogenesis in Drosophila, embryos undergo PM and actin remodeling in the form of successive rounds of furrow ingression and regression (Schejter and Wieschaus, 1993). Following fertilization, the first 13 cycles of mitosis proceed with no intervening cytokinesis. Instead, at mitotic cycles 1–9, nuclei divide in the embryo interior with no associated PM furrowing. At cycle 10 the nuclei move to the embryo periphery, and during interphase of cycles 10–14 cortical domes, called somatic buds, form over each nucleus. At the onset of mitosis, the margins of somatic buds ingress as short “metaphase furrows”, which separate cortically anchored spindles and insure the appropriate division of DNA between adjacent nuclei. By late mitosis these transient furrows completely regress. The result after 13 rapid mitotic cycles is a syncytial embryo filled with ~6000 nuclei.

Finally at interphase of mitotic cycle 14, the embryo completes a modified cytokinesis (Schejter and Wieschaus, 1993). During this process of cellularization, the somatic bud margins ingress between each nucleus. But rather than quickly regressing like transient metaphase furrows, cellularization furrows stably ingress and ultimately form a sheet of 40 μm tall adherent epithelial cells. The developmental switch that triggers the completion of cytokinesis at cycle 14 remains unclear. Since the entire process takes place during interphase, furrow stabilization and ingression is not likely to be regulated by cell cycle-dependent signals. Instead, expression of the zygotic genome starts just prior to the onset of cellularization and appears to differentially regulate the maternal, cellular machinery to build furrows that stably ingress. Specifically, expression of only a few zygotic gene-products, including *nullo*, *serendipity-α*, *slam* and *bottleneck* (Wieschaus, 1996), controls the maternal store of proteins by as yet poorly defined mechanisms so that cellularization is initiated and completed.

Furrow dynamics in Drosophila embryos have classically served as a model for cytoskeletal regulation, since microtubules largely direct actin rearrangements throughout the rounds of furrowing (Foe et al., 2000), and assembly of the F-actin/Myosin-2 furrow canals at the tips of cellularization furrows preface their sustained ingression (Grosshans et al., 2005; Padash Barmchi et al., 2005; Warn et al., 1980; Warn and Magrath, 1983). But the dramatic PM furrow dynamics suggest an additional regulatory function for the membrane trafficking machinery. Furthermore, while common machinery may initiate furrowing at both cellularization and the preceding mitotic cycles, the membrane requirements for sustained furrow ingression will necessarily vary from those of furrow regression. Comparing the mechanisms that generate ingression versus regression in these embryos, thus, affords a unique opportunity to understand how membrane trafficking is differentially regulated to achieve specific morphogenetic events.

PM growth at cellularization increases the embryonic surface by ~20-fold, and so intuitively establishes a role for exocytosis in this process. Exocytosed membrane inserts at specific sites along the cellularization furrow (Lecuit and Wieschaus, 2000), and is derived from both golgi compartments (Lee et al., 2003; Sisson et al., 2000) and recycling endosomes (Pelissier et al., 2003; Riggs et al., 2003). But whether endocytosis contributes to furrow ingression and/or regression in these embryos is an outstanding question. Mutant and dominant negative analysis, proteomics and drug studies have shown that endocytosis is required for the completion of cytokinesis in a variety of other cell types (Dhonukshe et al., 2006; Feng et al., 2002; Gerald et al., 2001; Niswonger and O’Halloran, 1997; Schweitzer et al., 2005; Skop et al., 2004; Thompson et al., 2002), and that membrane endocytosed from remote sites along the PM is delivered to the division plane via the endocytic pathway (Dhonukshe et al., 2006; Schweitzer et al., 2005). Thus, endocytosis may provide components to fuel PM growth at cytokinetic furrows. At cellularization furrows, the exocytosis of membrane derived from recycling endosomes similarly implies prior endocytosis. Consistent with this, ingression of cellularization furrows is arrested by

disrupting either Dynamin (Pelissier et al., 2003), which catalyzes vesicle scission from the PM and recycling endosomes, or Rab5 GTPase (Pelissier et al., 2003), which regulates early endosome dynamics. Furrow ingression also fails following perturbation of the Arfofilin-2 homolog Nuclear-fallout, or Rab11 GTPase, both of which regulate recycling endosome dynamics (Pelissier et al., 2003; Riggs et al., 2003). However, while endocytosis likely accompanies cellularization, it has not been directly observed, nor its location or timing well defined.

We approached the current study assuming that maternal machinery is developmentally controlled to convert transient furrows of the early mitotic cycles into stable, ingressing furrows at cellularization. We find that endocytosis is one target of this developmental control. Local endocytosis occurs where furrows first ingress throughout early development, but is differentially regulated by the zygotic gene product Nullo during cellularization. We show that *nullo* mutations impair endocytic dynamics such that furrows are unstable and regress. We propose that Nullo acts as a developmental switch at the onset of cellularization, targeting endocytosis and so directing the assembly of stable furrows that ingress to complete cellularization.

Results

Local endocytosis is controlled by cell cycle progression during the early mitotic cycles

Successive rounds of PM furrowing in the Drosophila embryo likely require that membrane trafficking be tightly controlled. During mitotic cycles 10–14, we observed that components of the endocytic machinery, including Dynamin, Clathrin light chain and Amphiphysin (Amph) localized to the margins of somatic buds and tips of metaphase furrows (Figures S1 and 1B). Strikingly, long thin Amph projections extended into the cytoplasm from bud margins and furrow tips (Figure 1B). Amph contains a membrane deforming Bin-Amph-Rvs domain, and as such induces the formation of membrane tubules from liposomes *in vitro* (Razzaq et al., 2001; Takei et al., 1999) and from the PM *in vivo* (Lee et al., 2002; Peter et al., 2004). During endocytosis this activity may constrict the neck between the PM and budding vesicle to aid membrane scission (Takei et al., 1999; Yoshida et al., 2004). Thus, Amph projections here may be membrane tubules, representing an intermediate of local endocytosis from furrow regions. Analysis of *en face* confocal images and volumetric renderings confirmed that Amph projections are tubules (Figures S2 and 3D; Movie S1). Amph tubules localized exclusively at PM regions where furrows form, and their appearance correlated with progression through the cell cycle (Figure 1B). That is, a small number of Amph tubules were seen at somatic bud margins during interphase, sharply increased at the tips of incipient metaphase furrows during prophase/metaphase, and then were completely absent at regressing furrows during telophase.

To ask how Amph tubules correlate with endocytosis in living embryos, we injected fluorophore-conjugated wheat-germ agglutinin (Alexa488-WGA) into the peri-vitelline space of cycle 10–13 embryos and then imaged at the embryo midsection by time-lapse confocal microscopy. Alexa488-WGA, which is a probe for glycosylated transmembrane proteins, bound rapidly to the cell surface immediate to the injection site (Lecuit and Wieschaus, 2000). When injected at interphase, Alexa488-WGA concentrated in surface patches at the bud margins (Figure 1C). These patches mark where metaphase furrows will ingress. When injected at interphase/prophase transition, Alexa488-WGA labeled metaphase furrows, concentrating at their tips. During prophase/metaphase, small numbers of Alexa488-WGA vesicles are released from these tips. Thus, endocytosis accompanies furrow ingression and coincides with the presence of Amph tubules observed in fixed tissue (Figures 1B and 1D; Movies S2 and S3). This prophase/metaphase distribution of Alexa488-WGA was followed by a dramatic wave of increased endocytosis that swept across the

embryo surface as the cortex was maximally displaced along the polar axis (Figure 1E; Movie S4). This displacement coincides with the anaphase/telophase transition when metaphase furrows regress (Figure S3; Movie S5 and S6). Thus, a burst of fast, vigorous endocytosis accompanies metaphase furrow regression, but is not detected by Amph tubules in fixed embryos. Since Amph tubules correspond with modest Alexa488-WGA endocytosis at furrow ingression rather than dramatic, fast endocytosis at regression, they may represent an endocytic intermediate that is more easily captured when endocytosis is ongoing, but somehow restrained. These trends were common to mitotic cycles 10–13, suggesting that endocytic dynamics are differentially controlled by cell cycle progression at times of furrow ingression versus regression in these early embryos.

Local endocytosis is controlled during cellularization

Since Amph tubules are associated with furrow ingression but not furrow regression during early mitotic cycles, endocytosis at ingression may be mechanistically distinct from that at regression. To further examine endocytosis accompanying furrow ingression, we looked for endocytosis at forming cellularization furrows. We visualized endocytosis in living embryos by injecting Alexa488-WGA into the peri-vitelline space of late cycle 13 embryos and then imaged at the embryo mid-section by time-lapse confocal microscopy. Again, Alexa488-WGA, bound rapidly to the cell surface immediate to the injection site (Figures 2B and 2C; Movie S7). As cellularization began Alexa488-WGA concentrated in surface patches that lengthened basally between the nuclei at speeds characteristic for early cellularization furrow ingression (Royou et al., 2004). Vesicles budded from Alexa488-WGA patches and were released into the cytoplasm (Figure 2B; Movie S6). Each patch gave rise to several vesicles over time (7.3 ± 0.4 vesicles/furrow). Once released into the cytoplasm, vesicles traveled in straight trajectories at 0.09 ± 0.004 μm/second to form a pad of bouncing Alexa488-WGA-labeled punctae just basal to the nuclei. In fixed embryos the punctae co-localized with FYVE-domain and Rab5 probes (Figures 2C and 2D; data not shown), which label early endosomes (Wucherpfennig et al., 2003). This indicates that endocytosed Alexa488-WGA can associate with early endosomes, although we have not yet resolved the dynamics of this association. (Thus, we use the term “vesicle” for Alexa488-WGA internalization in living embryos.)

As with embryos in the early mitotic cycles, we also looked for components of the endocytic machinery in cellularization furrows. Dynamin, Clathrin light chain and Amph concentrated at the tips of the forming furrows (Figures S4 and 3A; Leventis et al., 2001; Zelhof et al., 2001). Amph tubules extended from the furrow tips, but only at the onset of cellularization. This suggested that endocytic dynamics are controlled during cellularization. Quantification of projected cross-sections (Figure 3B) revealed that numerous Amph tubules are present as cellularization furrows first ingress, but are no longer detected by the time furrows reach 5 μm in length (Figure 3C). In living embryos, several Alexa488-WGA vesicles were released from furrows at the onset of cellularization, but their numbers diminished as cellularization proceeded (67% of vesicles formed before the furrow reached 3 μm length, n = 193 vesicles released from 25 furrows quantified to 5 μm length). These results indicate that local Amph-associated endocytosis is a general feature of furrow formation at cellularization as well as the mitotic cycles 10–13. Cell cycle progression appears to regulate endocytic dynamics in earlier embryos, such that restrained endocytosis during furrow ingression at prophase/metaphase is followed by fast, vigorous endocytosis during furrow regression at anaphase/telophase. At cellularization, cell cycle progression is unlikely to account for endocytic regulation since the process takes place entirely during interphase. Furthermore, there is no onset of fast endocytosis as cellularization furrows continue to ingress, and instead there appears to be a cessation of endocytosis once furrows reach 5 μm in length. Thus, some alternative regulator(s) must control endocytic dynamics at the beginning of cellularization.

Nullo is a developmental regulator of endocytic dynamics at cellularization

Cellularization furrows are stabilized at their tips by F-actin/Myosin-2 furrow canals, which are fully assembled once furrows reach 5 μm in length (Grosshans et al., 2005; Padash Barmchi et al., 2005). Furrow canals then insure sustained furrow ingression over an additional 30–35 μm to accomplish cellularization. Given that the timing of furrow canal assembly coincides with the cessation of endocytosis from furrow tips, we wondered whether any proteins involved in furrow canal assembly also control endocytic dynamics. Zygotic transcription starts just prior to cellularization and the zygotic gene product Nullo is required for furrow canal assembly. Nullo is first detected in mitotic cycle 13, peaks at the time of furrow canal assembly in early cycle 14 and is then degraded as cellularization proceeds (Postner and Wieschaus, 1994). Nullo concentrates in assembling furrow canals (Figure S5; Postner and Wieschaus, 1994), and *nullo* loss-of-function mutants (*nulloX*) fail to accumulate Myosin-2 at ~35% of their furrow canals from the beginning of cellularization (Figure S5; Simpson and Wieschaus, 1990).

To examine endocytic dynamics in these mutants, we first fixed *nulloX* embryos and stained for Amph tubules. Amph coated long tubules that extended from the furrow canal regions in *nulloX* embryos (Figure 4A). We quantified the number of tubules with respect to furrow length and found that unlike wild-type embryos where the Amph tubules were cleared by the time the ingressing furrow reached 5 μm, in *nulloX* embryos Amph tubules persisted until the furrow reached 10–20 μm in length (Fig. 4C).

To better understand the basis of the *nulloX* phenotype, we injected Alexa488-WGA into the perivitelline space of living *nulloX* embryos. Confocal time-lapse imaging showed that Alexa488-WGA concentrated in surface patches from which furrows ingressed basally at rates comparable to wild-type (0.5 ± 0.04 μm/minute; Figure 4B; Movie S8). Alexa488-WGA vesicles budded from the patches, but the number of vesicles released was significantly less than in wild-type (3.1 ± 0.3 vesicles/furrow; $p < 1.8 \times 10^{-6}$). Also, vesicle release from the PM was ~3 times slower than in wild-type embryos (108.9 ± 9.7 seconds elapsed between bud appearance to vesicle release in *nulloX* versus 38.1 ± 2.4 seconds in wild-type; $p < 1.7 \times 10^{-8}$). In the most dramatic examples, budding vesicles were actually distended into long tubules before release into the cytoplasm (Figure 4B; Movie S8). Since prolonged release permitted the entry of more membrane per vesicle, early endosomes were sometimes enlarged in nulloX versus wild-type embryos (Figure S6). Once released *nulloX* vesicles moved into the cytoplasm at speeds equal to wild-type (0.082 ± 0.02 μm/second).

Slower release of vesicles from the PM and frequent distension of budding vesicles into membrane tubules in living *nulloX* embryos could indicate that Nullo functions upstream of endocytic scission, and might explain why increased numbers of Amph tubules are seen in fixed mutants (Figure 4A). To confirm this, we perturbed scission using a temperature-sensitive allele of *dynamin* (*shibire; shi*^{ts}). We quantified the number of Amph tubules in *shi*^{ts} embryos incubated at permissive versus restrictive temperatures. Dynamin perturbation by heat-shock yielded numerous long Amph tubules that persisted until furrows reached 10–20 μm in length (Figures 4D–F), resembling the abnormal dynamics seen for *nulloX* mutants (Figure 4A and 4C). Thus, we conclude that scission is impaired in *nulloX* mutants such that vesicles bud from the PM, but remain tethered there for some prolonged period during which they can distend into tubules.

Nullo controls endocytic dynamics via cortical F-actin

Dynamin can act directly to catalyze scission, but may also contribute indirectly by promoting local F-actin assembly around the neck of a budding vesicle (Kaksonen et al., 2006). In mammalian cells (Merrifield et al., 2002; Merrifield et al., 2004; Yarar et al., 2005,

2007) and yeast (Gachet and Hyams, 2005; Kaksonen et al., 2003; Kaksonen et al., 2005), elegant live-imaging has revealed that bursts of F-actin assembly accompany this late step of endocytosis, and F-actin perturbation compromises the efficiency of scission (Kaksonen et al., 2006). Since scission of endocytic vesicles from furrows was impaired in *nulloX* mutants, we wondered whether these embryos have global F-actin defects.

Indeed, we found that all furrow canals in *nulloX* embryos have significantly reduced levels of F-actin compared to wild-type from the start of cellularization (Figures 5A and 5B; $p < 5.0 \times 10^{-5}$). In contrast to Myosin-2, which was missing from a fraction of furrows, F-actin was reduced at every furrow that was maintained in *nulloX* embryos. This is consistent with the appearance of endocytic defects at every furrow and suggests a primary role for Nullo in controlling cortical F-actin accumulation. We also drove *nullo* over-expression under control of the maternal *tubulin* promoter in cellularizing embryos using the UAS-GAL4 system (Sullivan et al., 2000). Furrow canals in *nullo* gain-of-function embryos have increased levels of F-actin compared to wild-type throughout cellularization (Figures 5C and 5D). However, this increase is only statistically significant early in cellularization when furrow lengths measure from 5–6 μm ($p < 9 \times 10^{-4}$), most strongly supporting Nullo regulation of actin at early cellularization.

To confirm that *nullo* gain-of-function increases F-actin levels, we also expressed *nullo* in a stripe of anterior cells in the imaginal wing-disc epithelium under control of the *patched* promoter using the UAS-GAL4 system (Figures 5E and 5F). These wing-discs showed a stripe of ectopic F-actin corresponding to the stripe of Nullo expression. Projected Z-sections confirmed that the ectopic actin was largely restricted to the basal/lateral cortex of these columnar epithelial cells where ectopic Nullo levels were highest (Figure 5E). Thus, Nullo can interface with proteins across tissue types to positively regulate F-actin levels at specific regions of the cortex.

Since actin plays an essential role in endocytic scission (Kaksonen et al., 2006), Nullo may aid scission via its regulation of F-actin. To test this, we generically reduced the levels of F-actin by Cytochalasin-D (Cyto-D) treatment and looked for endocytosis defects. Wild-type, cycle 14 embryos were permeabilized and treated with Cyto-D, and after fixation and staining the number of Amph-tubules were quantified. We chose a low dose of Cyto-D compared to that previously used in permeabilized embryos with the intention of reducing but not completely disrupting F-actin (Harris and Peifer, 2005; Townsley and Bienz, 2000). Following treatment with Cyto-D, embryos had sharply increased numbers of Amph-tubules (Figure 6A; compare 86.5 ± 3.7 tubules per Cyto-D embryo to 7.1 ± 0.8 tubules per DMSO control at furrow lengths of 5 μm; $p < 2.6 \times 10^{-12}$). Cyto-D induced membrane tubulation was most severe in very early cellularization furrows (< 5 μm in length), to the extent that furrows appeared to “disintegrate” into snarls of many tubules (Figure 6A). This early sensitivity to Cyto-D strongly supports a role for F-actin regulation of endocytic dynamics at the beginning of cellularization when furrows are just forming.

We also co-injected Alexa488-WGA with Cyto-D into the peri-vitelline space of living embryos, and captured time-lapse confocal images at the embryo midsection. Results were somewhat variable, which we attribute to the differential diffusion of the drug through the peri-vitelline space. This variability precluded reliable quantification in living embryos. Nonetheless, vesicle release from the PM was prolonged in Cyto-D treated embryos such that persistent membrane tubules formed (Figure 6A; see Movie S9). We did not detect any increase in the number of vesicles formed from a given Alexa488-WGA surface patch in Cyto-D treated embryos. Thus, as in *nulloX* mutants, Cyto-D induces membrane tubules, but not because the rate of vesicle budding is increased. Instead, membrane tubules are the intermediate formed following vesicle budding but preceding scission. These results

strongly support that Nullo controls scission dynamics at the beginning of cellularization via F-actin.

Endocytic dynamics are controlled to assemble stable furrow canals

We have shown that Nullo controls local endocytosis at the tips of incipient cellularization furrows, where actin/Myosin-2 furrow canals assemble. Since Nullo is required for furrow canal assembly, we wondered whether the regulation of endocytosis might be critical for proper furrow canal assembly and, consequently, stable furrow ingression. In *nulloX* embryos, we saw several furrow canal components incorporated into Amph-tubules, including the Septin Peanut (Fares et al., 1995), tyrosine-phosphorylated proteins (Thomas and Wieschaus, 2004), and the PDZ-containing scaffold protein DPATJ (Lecuit et al., 2002). DPATJ accumulation in Amph-tubules was especially prominent and could be clearly seen in Z-sections (Figure 7A). Furthermore, levels of DPATJ were obviously increased at early endosomes in *nulloX* mutants compared to wild-type (Figures 7A and S7). Strikingly, the components that entered Amph tubules in *nulloX* mutants were also depleted from some furrow canals, and furrows were absent at these sites (Figures 7B and 7C). Thus, reduced actin and impaired scission at every furrow canal appears to affect individual furrows to varying extents. That is, when membrane tubules are persistently tethered to the PM, they can non-specifically incorporate furrow canal components before being released into the cytoplasm. This depletes components from furrow canals and stochastically precipitates furrow failures where the depletion is most severe. This explains discontinuities in, but not complete ablation of, the furrow canal network in *nulloX* embryos. It is consistent with a primary role for Nullo in controlling endocytosis at the onset of cellularization, and suggests that this control is essential for stable furrow formation.

Discussion

Early morphogenetic events are accomplished by maternal cellular machinery that is developmentally controlled by expression of the zygotic genome (Wieschaus, 1996). We find that the zygotic gene-product Nullo acts as a developmental switch at cycle 14 and targets the endocytic machinery to cellularize the embryo. Here we assayed endocytic dynamics by following WGA internalization in living embryos and Amph tubulation in fixed embryos. We find that WGA is a general marker for endocytosis, while Amph tubules are more specifically associated with the initial ingression of PM furrows. Several findings support that these Amph tubules are endocytic intermediates: First, their structure is tubular rather than sheet-like, consistent with a role in endocytosis. Second, perturbation of Dynamin, a catalyst of endocytic scission, increases the number of Amph tubules at cellularization furrows. Third, in living *nulloX* and Cyto-D treated embryos, WGA is internalized in long, PM-tethered tubules that resemble Amph tubules. Fourth, DPATJ enters Amph tubules in *nulloX* embryos, and accumulates at early endosomes. We have, thus, used Amph tubules as quantifiable reporters of endocytosis at furrows.

The membrane furrows that form during the early mitotic cycles regress, while those that form at cellularization stably ingress. We propose that endocytosis is differentially controlled to achieve these distinct morphogenetic events. During the mitotic cycles, metaphase furrows are transient, ingressing only ~5 μm before completely regressing. We find that restrained endocytosis, detected by both WGA internalization and Amph tubules, accompanies the initial furrow ingression that occurs at prophase/metaphase. This is followed by a fast wave of vigorous WGA endocytosis that traverses the embryo surface when metaphase furrows regress at anaphase/telophase. The endocytosis accompanying furrow regression is not associated with high levels of Amph tubules. While this endocytosis may not recruit Amph, we favor a model whereby endocytic scission is more efficient at this time, precluding the capture of tubule intermediates by fixation. Thus, endocytosis at furrow

regression may be mechanistically distinct from endocytosis at furrow ingression. It may also be functionally distinct and could even drive furrow regression, as endocytosis adjusts the surface area of both motile and dividing cells (Boucrot and Kirchhausen, 2007; Traynor and Kay, 2007). So throughout the early mitotic cycles, alternating and distinct endocytic dynamics are regulated by cell cycle progression and correlate with specific furrow events.

At the onset of cellularization, furrows form in a way that resembles metaphase furrows, but then assemble furrow canals that stabilize the furrow and sustain ingression over ~40 μm. We find that endocytosis, marked by both WGA internalization and Amph tubules, also accompanies the initial ingression of cellularization furrows, but ceases by the time furrows reach 5 μm in length and furrow canals fully assemble. Since cellularization occurs during interphase, cell cycle progression cannot regulate this endocytosis. Instead, zygotic expression of Nullo aids endocytic scission, and this has the effect of limiting membrane dynamics at the tip of the incipient cellularization furrow, so that proteins, including Myosin-2, Septin, and DPATJ, that concentrate there are retained there. As a result, furrow canals assemble and stabilized furrows ingress to cellularize the embryo. Thus, Nullo regulation of endocytic dynamics could promote the developmental transition from transient furrowing that maintains the syncytium to stable furrowing that generates the primary epithelial cell sheet.

Nullo activity facilitates endocytic scission such that budding vesicles are rapidly released from the PM. When scission is impaired some budding vesicles are distended into long Amph tubules that remain persistently tethered to the PM. This phenotype is mimicked when F-actin levels are reduced with Cyto-D, and Nullo regulates cortical F-actin. Thus, we suggest that Nullo aids scission via its regulation of F-actin. How Nullo regulates actin remains elusive as it is a small (213 amino acids), highly basic (pI 11.4), myristoylated protein with no readily identifiable globular domains to suggest interaction partners. Instead, sequence composition and hydropathy character suggest that Nullo is “natively unfolded”, containing 63% disorder promoting amino acids (T, R, G, Q, S, N, P, D, E, and K) over its entire length (Williams et al., 2001) and a disordered run of 50 consecutive amino acids as predicted by PONDR analysis (L136 - A185). Other disordered proteins have been identified that control F-actin organization, such as MARCKs, MARCKs-related proteins and GAP43 (Arbuzova et al., 2002; Larsson, 2006), either by direct interaction with actin or by locally sequestering the actin-regulator PIP_2 within the PM. While sequence comparison and lack of characteristic, acidic regions does not suggest that Nullo is MARCKs-related, we find that Nullo interacts with PIP_2 in *in vitro* binding assays (Sokac and Wieschaus, unpublished data). Nullo may then concentrate PIP_2 locally to regulate actin and/or to couple actin to components of the endocytic machinery that also interact with PIP_2 at the PM (Di Paolo and De Camilli, 2006).

Nullo may aid endocytic scission via F-actin by either active or passive mechanisms. In yeast, F-actin actively drives endocytic scission by exerting polymerization and myosin-based forces to lengthen, and eventually break, the budding vesicle neck (Kaksonen et al., 2003; Kaksonen et al., 2005; Sun et al., 2006). In Drosophila hemocytes and mammalian cells, F-actin also contributes to a late step in endocytosis that just precedes vesicle release, and may be either bud invagination or scission (Kochubey et al., 2006; Merrifield et al., 2002; Merrifield et al., 2004; Yarar et al., 2005, 2007). Additionally, cortical F-actin passively regulates endocytic dynamics by reinforcing the PM and so antagonizing PM deformation. In the case of BAR domain activity, drug mediated reduction of F-actin levels enhances PM tubulation (Itoh et al., 2005). Reduced levels of cortical F-actin in *nulloX* mutants result in the appearance of more Amph tubules. But we find that fewer vesicles are released in living *nulloX* embryos, and that Amph tubulation does not expand to regions beyond the furrow, arguing that there is not more endocytosis in mutants. Thus, impaired

scission generates the appearance of more tubules, and we find that it takes almost three times longer for budding vesicles to release from the PM in *nulloX* versus wild-type embryos. Consistently, dynamin defects enhance PM tubulation in cultured cells and BAR-induced membrane tubulation is antagonized by co-expression of dynamin (Itoh et al., 2005). So Nullo may regulate a population of F-actin that either actively aids scission, or stiffens the cortex and somehow contributes to endocytosis (ie. if breaking the bud neck is aided by the PM being under cortically-maintained tension).

Our analysis strongly supports that membrane trafficking is differentially controlled at specific sites and times within embryos to achieve distinct morphogenetic events. This was previously suggested for fly embryos by the membrane-labeling analysis of Lecuit and Wieschaus (2000), which demonstrated that exocytosis occurs at specific sites along cellularization furrows and so helps establish apical/basal polarity in these cells. Two additional observations were made at that time that are relevant to the results described here: First, in the earlier study membrane labeling of the furrow canal was only possible at very early cellularization. After that time the furrow canal persisted as a stable membrane compartment where no new membrane was either added or taken away. Our data also supports that membrane turnover at the furrow canal region is restricted to the very beginning of cellularization. In fact, we now find that endocytic dynamics are tightly controlled there to establish and/or maintain the concentration of proteins at the furrow canal. Second, in the previous study it was observed that membrane label was cleared from the apical PM, and was suggested that clearing is mediated by endocytosis. At furrow lengths > 5 μm, we also see WGA vesicles moving away from the apical PM. But when our peri-vitelline injections were done with higher lectin concentrations and at furrow lengths < 5 μm, they revealed WGA endocytosis from the tips of incipient furrows. In fixed embryos where spatial resolution is better, Amph tubules clearly extend only from furrow tips. Thus, our analysis shows that in addition to apical endocytosis, local endocytosis also occurs where furrows first ingress.

During cytokinesis in some mammalian cells (Schweitzer et al., 2005) and in plants (Dhonukshe et al., 2006), membrane endocytosed at sites remote from the furrow is later delivered to the division plane via the endocytic pathway. At cellularization furrows in the fly embryo the exocytosis of membrane derived from recycling endosomes suggests a similar pathway. In these cases, endocytosis from one site can provide a store of membrane to feed growth somewhere else. But our observation that endocytosis occurs at the furrow itself is counterintuitive since endocytosis would be expected to reduce surface area while furrow ingression requires surface expansion. Nonetheless, there are now several reports that endocytic proteins including Clathrin, Clathrin adaptor-2 and Dynamin concentrate in cytokinesis furrows (Albertson et al., 2005). In addition, endocytosis has been directly visualized at furrows in dividing Zebrafish embryos (Feng et al., 2002), cultured cells (Sweitzer and Hinshaw, 1998; Warner et al., 2006) and fission yeast (Gachet and Hyams, 2005), although the function of this endocytosis remains unclear.

We report that endocytosis occurs at the tips of both metaphase and cellularization furrows when the furrows are first ingressing, suggesting that it confers some temporally and spatially specific function. Both the PM and actin are significantly remodeled at these sites as furrows form. At the onset of cellularization in particular, the F-actin/Myosin-2 furrow canals are assembling at this place and time. Actin remodeling is intimately coupled to endocytosis in other cell types (Smythe and Ayscough, 2006): Endocytic proteins control actin dynamics and actin binding proteins are required for endocytosis. Also, endocytic and actin binding proteins are regulated by the same phosphoinositide pools at the PM (Di Paolo and De Camilli, 2006). It follows that local endocytosis could influence local actin organization during furrow formation in fly embryos. Here we show that actin conversely

provides developmental regulation of endocytic dynamics. This analysis leads us to speculate that the coupled regulation of actin and endocytosis can effectively coordinate actin/PM remodeling to drive furrow dynamics, and so shape cells during morphogenesis.

Experimental Procedures

Embryo manipulation, fixation and antibody staining

Information regarding fly stocks is detailed in the Supplemental Experimental Procedures.

For *shi*^{ts1} heat shock, embryos were incubated at 32°C for 20 minutes.

For permeabilization, the protocol of Townsley and Bienz, 2000 was followed and embryos incubated for 6 minutes in 1 μg ml^{-1} Cyto-D (reconstituted in DMSO).

For immunofluorescence, embryos were either fixed in boiling salt buffer (Muller and Wieschaus, 1996) or 4% formaldehyde/0.1 M phosphate buffer, pH 7.4. Wing discs were fixed in 4% formaldehyde/0.1 M phosphate buffer, pH 7.4. Antibody concentrations are listed in Table S1.

For F-actin detection, embryos were fixed in 18.5% formaldehyde/0.1 M phosphate buffer, pH 7.4:heptane, and hand peeled for staining with Alexa488-phalloidin (5U ml^{-1}, Invitrogen-Molecular Probes).

Confocal images were collected on a Zeiss LSM 510 microscope (Carl Zeiss, Inc., Thornwood, NY) with a numerical aperture 1.2, 40X objective lens.

Live-imaging

For the endocytosis assay, embryos were dechorionated, mounted to a coverslip with heptane glue, desiccated and then submerged in halocarbon oil 700. Approximately 50 pl of Alexa488-WGA or Alexa546-WGA (0.7 mg ml^{-1} in PBS; Molecular Probes) was injected into the peri-vitelline space (Stein et al., 1991). The *nulloX* embryos were not genotyped, so results were confirmed by dsRNA depletion. Early embryos (≤ 30 minutes post-egg laying) were injected with 40 pl of *nullo* dsRNA (4 μM) prior to peri-vitelline injection. For drug treatment, 2.5 μg ml^{-1} Cyto-D was co-injected with the Alexa488-WGA. Confocal images were collected at the embryo equator, at 10 second intervals on a Nikon TE300 microscope (Nikon, Melville, NY)/MRC1024 system (Bio-Rad, Hercules, CA) with a numerical aperture 1.3, 40X objective.

Image analysis, quantification and statistics

For F-actin fluorescence intensity in furrow canals, three confocal Z-sections were collected at the dorsal equator of each embryo. All laser settings were constant. Images were analyzed in MATLAB (Image Processing Toolbox, The MathWorks, Natick, MA) as follows: First, average furrow length per embryo was calculated based on five furrows per embryo. Second, furrow canals were identified by thresholding and then hand-selected to eliminate falsely identified objects (to verify thresholding, we tested a range of values, all giving the same trend). Mean intensity was calculated per image and then averaged for the three images, such that each data point on the plots represents ~100 furrow canals from one embryo. Data was fitted to a polynomial of the second degree. Trend maintained in 3 independent experiments.

For furrow ingression and vesicle motility rates in living embryos, kymographs were generated from time-lapse sequences in MATLAB. Data presented as mean ± SEM, n = 15 furrows or vesicles, from 3 embryos.

For vesicle budding dynamics, rare cases where tubules persisted > 4 minutes were not included in the quantification. Data presented as mean ± SEM, n = 50 vesicles, from 3 embryos.

For membrane tubules in fixed embryos, Z-sections were projected from 512 ×512 confocal image stacks with Volocity software (Improvision Inc., Waltham, MA) at every 50-pixel interval along the Y-axis. Thus, ~180 furrow canals were examined per embryo. Tubules that extended below the furrow canals were counted. Plotted data for wild-type and *nulloX* mutants was fitted to an exponential. Trend maintained in 2 independent experiments. The shi^{ts}, Cyto-D and DMSO data presented as mean ± SEM, n = 15 embryos and trend maintained in 3 independent experiments.

All MATLAB source code is available upon request.

Nullo sequence analysis

Nullo amino acid sequences were analyzed for disorder using the default settings of the PONDR software. Access to PONDR was provided by Molecular Kinetics (Indianapolis, IN).

Supplemental Data

Refer to Web version on PubMed Central for supplementary material.

Acknowledgments

We warmly thank Ido Golding for writing the MATLAB source code; Carlos-Vanario Alonso, Manzoor Bhat, Gabrielle Boulianne, Marcos González-Gaitán, Manos Mavrakis, Harvey McMahon and John Reinitz for providing antibodies and flies; Joe Goodhouse for assisting with microscopy; and Bill Bement, Natalie Denef, Stefano De Renzis and Adam Martin for discussing results. E.W. is an Investigator of the Howard Hughes Medical Institute. Support for A.M.S. provided by a Post-Doctoral National Research Service Award from the National Institutes of Health.

References

Albertson R, Riggs B, Sullivan W. Membrane traffic: a driving force in cytokinesis. Trends in cell biology 2005;15:92–101. [PubMed: 15695096]

Arbuzova A, Schmitz AA, Vergeres G. Cross-talk unfolded: MARCKS proteins. Biochem J 2002;362:1–12. [PubMed: 11829734]

Boucrot E, Kirchhausen T. Endosomal recycling controls plasma membrane area during mitosis. Proc Natl Acad Sci U S A 2007;104:7939–7944. [PubMed: 17483462]

Chang HC, Newmyer SL, Hull MJ, Ebersold M, Schmid SL, Mellman I. Hsc70 is required for endocytosis and clathrin function in Drosophila. J Cell Biol 2002;159:477–487. [PubMed: 12427870]

Dhonukshe P, Baluska F, Schlicht M, Hlavacka A, Samaj J, Friml J, Gadella TW Jr. Endocytosis of cell surface material mediates cell plate formation during plant cytokinesis. Dev Cell 2006;10:137–150. [PubMed: 16399085]

Di Paolo G, De Camilli P. Phosphoinositides in cell regulation and membrane dynamics. Nature 2006;443:651–657. [PubMed: 17035995]

Dudu V, Pantazis P, Gonzalez-Gaitan M. Membrane traffic during embryonic development: epithelial formation, cell fate decisions and differentiation. Current opinion in cell biology 2004;16:407–414. [PubMed: 15261673]

Emery G, Knoblich JA. Endosome dynamics during development. Current opinion in cell biology 2006;18:407–415. [PubMed: 16806877]

Fares H, Peifer M, Pringle JR. Localization and possible functions of Drosophila septins. Mol Biol Cell 1995;6:1843–1859. [PubMed: 8590810]

Feng B, Schwarz H, Jesuthasan S. Furrow-specific endocytosis during cytokinesis of zebrafish blastomeres. Experimental cell research 2002;279:14–20. [PubMed: 12213209]

Foe VE, Field CM, Odell GM. Microtubules and mitotic cycle phase modulate spatiotemporal distributions of F-actin and myosin II in Drosophila syncytial blastoderm embryos. Development 2000;127:1767–1787. [PubMed: 10751167]

Gachet Y, Hyams JS. Endocytosis in fission yeast is spatially associated with the actin cytoskeleton during polarised cell growth and cytokinesis. J Cell Sci 2005;118:4231–4242. [PubMed: 16141239]

Gerald NJ, Damer CK, O'Halloran TJ, De Lozanne A. Cytokinesis failure in clathrin-minus cells is caused by cleavage furrow instability. Cell motility and the cytoskeleton 2001;48:213–223. [PubMed: 11223952]

Grosshans J, Wenzl C, Herz HM, Bartoszewski S, Schnorrer F, Vogt N, Schwarz H, Muller HA. RhoGEF2 and the formin Dia control the formation of the furrow canal by directed actin assembly during Drosophila cellularisation. Development 2005;132:1009–1020. [PubMed: 15689371]

Harris TJ, Peifer M. The positioning and segregation of apical cues during epithelial polarity establishment in Drosophila. J Cell Biol 2005;170:813–823. [PubMed: 16129788]

Hunter C, Wieschaus E. Regulated expression of nullo is required for the formation of distinct apical and basal adherens junctions in the Drosophila blastoderm. J Cell Biol 2000;150:391–401. [PubMed: 10908580]

Itoh T, De Camilli P. BAR, F-BAR (EFC) and ENTH/ANTH domains in the regulation of membrane-cytosol interfaces and membrane curvature. Biochimica et biophysica acta 2006;1761:897–912. [PubMed: 16938488]

Itoh T, Erdmann KS, Roux A, Habermann B, Werner H, De Camilli P. Dynamin and the actin cytoskeleton cooperatively regulate plasma membrane invagination by BAR and F-BAR proteins. Dev Cell 2005;9:791–804. [PubMed: 16326391]

Kaksonen M, Sun Y, Drubin DG. A pathway for association of receptors, adaptors, and actin during endocytic internalization. Cell 2003;115:475–487. [PubMed: 14622601]

Kaksonen M, Toret CP, Drubin DG. A modular design for the clathrin- and actin-mediated endocytosis machinery. Cell 2005;123:305–320. [PubMed: 16239147]

Kaksonen M, Toret CP, Drubin DG. Harnessing actin dynamics for clathrin-mediated endocytosis. Nat Rev Mol Cell Biol 2006;7:404–414. [PubMed: 16723976]

Kochubey O, Majumdar A, Klingauf J. Imaging clathrin dynamics in Drosophila melanogaster hemocytes reveals a role for actin in vesicle fission. Traffic (Copenhagen, Denmark) 2006;7:1614–1627.

Larsson C. Protein kinase C and the regulation of the actin cytoskeleton. Cell Signal 2006;18:276–284. [PubMed: 16109477]

Lecuit T, Samanta R, Wieschaus E. slam encodes a developmental regulator of polarized membrane growth during cleavage of the Drosophila embryo. Dev Cell 2002;2:425–436. [PubMed: 11970893]

Lecuit T, Wieschaus E. Polarized insertion of new membrane from a cytoplasmic reservoir during cleavage of the Drosophila embryo. J Cell Biol 2000;150:849–860. [PubMed: 10953008]

Lee E, Marcucci M, Daniell L, Pypaert M, Weisz OA, Ochoa GC, Farsad K, Wenk MR, De Camilli P. Amphiphysin 2 (Bin1) and T-tubule biogenesis in muscle. Science 2002;297:1193–1196. [PubMed: 12183633]

Lee OK, Frese KK, James JS, Chadda D, Chen ZH, Javier RT, Cho KO. Discs-Large and Strabismus are functionally linked to plasma membrane formation. Nat Cell Biol 2003;5:987–993. [PubMed: 14562058]

Leventis PA, Chow BM, Stewart BA, Iyengar B, Campos AR, Boulianne GL. Drosophila Amphiphysin is a post-synaptic protein required for normal locomotion but not endocytosis. Traffic (Copenhagen, Denmark) 2001;2:839–850.

Marco E, Wedlich-Soldner R, Li R, Altschuler SJ, Wu LF. Endocytosis optimizes the dynamic localization of membrane proteins that regulate cortical polarity. Cell 2007;129:411–422. [PubMed: 17448998]

Men S, Boutte Y, Ikeda Y, Li X, Palme K, Stierhof YD, Hartmann MA, Moritz T, Grebe M. Sterol-dependent endocytosis mediates post-cytokinetic acquisition of PIN2 auxin efflux carrier polarity. Nat Cell Biol. 2008

Merrifield CJ, Feldman ME, Wan L, Almers W. Imaging actin and dynamin recruitment during invagination of single clathrin-coated pits. Nat Cell Biol 2002;4:691–698. [PubMed: 12198492]

Merrifield CJ, Qualmann B, Kessels MM, Almers W. Neural Wiskott Aldrich Syndrome Protein (N-WASP) and the Arp2/3 complex are recruited to sites of clathrin-mediated endocytosis in cultured fibroblasts. European journal of cell biology 2004;83:13–18. [PubMed: 15085951]

Muller HA, Wieschaus E. armadillo, bazooka, and stardust are critical for early stages in formation of the zonula adherens and maintenance of the polarized blastoderm epithelium in Drosophila. J Cell Biol 1996;134:149–163. [PubMed: 8698811]

Niswonger ML, O'Halloran TJ. A novel role for clathrin in cytokinesis. Proc Natl Acad Sci U S A 1997;94:8575–8578. [PubMed: 9238018]

Padash Barmchi M, Rogers S, Hacker U. DRhoGEF2 regulates actin organization and contractility in the Drosophila blastoderm embryo. J Cell Biol 2005;168:575–585. [PubMed: 15699213]

Pelissier A, Chauvin JP, Lecuit T. Trafficking through Rab11 endosomes is required for cellularization during Drosophila embryogenesis. Curr Biol 2003;13:1848–1857. [PubMed: 14588240]

Peter BJ, Kent HM, Mills IG, Vallis Y, Butler PJ, Evans PR, McMahon HT. BAR domains as sensors of membrane curvature: the amphiphysin BAR structure. Science 2004;303:495–499. [PubMed: 14645856]

Postner MA, Wieschaus EF. The nullo protein is a component of the actin-myosin network that mediates cellularization in Drosophila melanogaster embryos. J Cell Sci 1994;107(Pt 7):1863–1873. [PubMed: 7983153]

Razzaq A, Robinson IM, McMahon HT, Skepper JN, Su Y, Zelhof AC, Jackson AP, Gay NJ, O'Kane CJ. Amphiphysin is necessary for organization of the excitation-contraction coupling machinery of muscles, but not for synaptic vesicle endocytosis in Drosophila. Genes Dev 2001;15:2967–2979. [PubMed: 11711432]

Riggs B, Rothwell W, Mische S, Hickson GR, Matheson J, Hays TS, Gould GW, Sullivan W. Actin cytoskeleton remodeling during early Drosophila furrow formation requires recycling endosomal components Nuclear-fallout and Rab11. J Cell Biol 2003;163:143–154. [PubMed: 14530382]

Royou A, Field C, Sisson JC, Sullivan W, Karess R. Reassessing the role and dynamics of nonmuscle myosin II during furrow formation in early Drosophila embryos. Mol Biol Cell 2004;15:838–850. [PubMed: 14657248]

Schejter ED, Wieschaus E. Functional elements of the cytoskeleton in the early Drosophila embryo. Annu Rev Cell Biol 1993;9:67–99. [PubMed: 8280474]

Schweitzer JK, Burke EE, Goodson HV, D'Souza-Schorey C. Endocytosis resumes during late mitosis and is required for cytokinesis. J Biol Chem 2005;280:41628–41635. [PubMed: 16207714]

Simpson L, Wieschaus E. Zygotic activity of the nullo locus is required to stabilize the actin-myosin network during cellularization in Drosophila. Development 1990;110:851–863. [PubMed: 2088725]

Sisson JC, Field C, Ventura R, Royou A, Sullivan W. Lava lamp, a novel peripheral golgi protein, is required for Drosophila melanogaster cellularization. J Cell Biol 2000;151:905–918. [PubMed: 11076973]

Skop AR, Liu H, Yates J 3rd, Meyer BJ, Heald R. Dissection of the mammalian midbody proteome reveals conserved cytokinesis mechanisms. Science 2004;305:61–66. [PubMed: 15166316]

Smythe E, Ayscough KR. Actin regulation in endocytosis. J Cell Sci 2006;119:4589–4598. [PubMed: 17093263]

Stein D, Roth S, Vogelsang E, Nusslein-Volhard C. The polarity of the dorsoventral axis in the Drosophila embryo is defined by an extracellular signal. Cell 1991;65:725–735. [PubMed: 1904007]

Sullivan, W.; Ashburner, M.; Hawley, RS. ebrary Inc. Drosophila protocols. Cold Spring Harbor, N.Y: Cold Spring Harbor Laboratory Press; 2000.

Sun Y, Martin AC, Drubin DG. Endocytic internalization in budding yeast requires coordinated actin nucleation and myosin motor activity. Dev Cell 2006;11:33–46. [PubMed: 16824951]

Sweitzer SM, Hinshaw JE. Dynamin undergoes a GTP-dependent conformational change causing vesiculation. Cell 1998;93:1021–1029. [PubMed: 9635431]

Takei K, Slepnev VI, Haucke V, De Camilli P. Functional partnership between amphiphysin and dynamin in clathrin-mediated endocytosis. Nat Cell Biol 1999;1:33–39. [PubMed: 10559861]

Thomas JH, Wieschaus E. src64 and tec29 are required for microfilament contraction during Drosophila cellularization. Development 2004;131:863–871. [PubMed: 14736750]

Thompson HM, Skop AR, Euteneuer U, Meyer BJ, McNiven MA. The large GTPase dynamin associates with the spindle midzone and is required for cytokinesis. Curr Biol 2002;12:2111–2117. [PubMed: 12498685]

Townsley FM, Bienz M. Actin-dependent membrane association of a Drosophila epithelial APC protein and its effect on junctional Armadillo. Curr Biol 2000;10:1339–1348. [PubMed: 11084333]

Traynor D, Kay RR. Possible roles of the endocytic cycle in cell motility. J Cell Sci 2007;120:2318–2327. [PubMed: 17606987]

Warn RM, Bullard B, Magrath R. Changes in the distribution of cortical myosin during the cellularization of the Drosophila embryo. Journal of embryology and experimental morphology 1980;57:167–176. [PubMed: 6776222]

Warn RM, Magrath R. F-actin distribution during the cellularization of the Drosophila embryo visualized with FL-phalloidin. Experimental cell research 1983;143:103–114. [PubMed: 6825714]

Warner AK, Keen JH, Wang YL. Dynamics of membrane clathrin-coated structures during cytokinesis. Traffic (Copenhagen, Denmark) 2006;7:205–215.

Wieschaus E. Embryonic transcription and the control of developmental pathways. Genetics 1996;142:5–10. [PubMed: 8770580]

Wieschaus E, Sweeton D. Requirements for X-linked zygotic gene activity during cellularization of early Drosophila embryos. Development 1988;104:483–493. [PubMed: 3256473]

Williams RM, Obradovi Z, Mathura V, Braun W, Garner EC, Young J, Takayama S, Brown CJ, Dunker AK. The protein non-folding problem: amino acid determinants of intrinsic order and disorder. Pac Symp Biocomput 2001:89–100. [PubMed: 11262981]

Wucherpfennig T, Wilsch-Brauninger M, Gonzalez-Gaitan M. Role of Drosophila Rab5 during endosomal trafficking at the synapse and evoked neurotransmitter release. J Cell Biol 2003;161:609–624. [PubMed: 12743108]

Yarar D, Waterman-Storer CM, Schmid SL. A dynamic actin cytoskeleton functions at multiple stages of clathrin-mediated endocytosis. Mol Biol Cell 2005;16:964–975. [PubMed: 15601897]

Yarar D, Waterman-Storer CM, Schmid SL. SNX9 couples actin assembly to phosphoinositide signals and is required for membrane remodeling during endocytosis. Dev Cell 2007;13:43–56. [PubMed: 17609109]

Yoshida Y, Kinuta M, Abe T, Liang S, Araki K, Cremona O, Di Paolo G, Moriyama Y, Yasuda T, De Camilli P, et al. The stimulatory action of amphiphysin on dynamin function is dependent on lipid bilayer curvature. The EMBO journal 2004;23:3483–3491. [PubMed: 15318165]

Zelhof AC, Bao H, Hardy RW, Razzaq A, Zhang B, Doe CQ. Drosophila Amphiphysin is implicated in protein localization and membrane morphogenesis but not in synaptic vesicle endocytosis. Development 2001;128:5005–5015. [PubMed: 11748137]

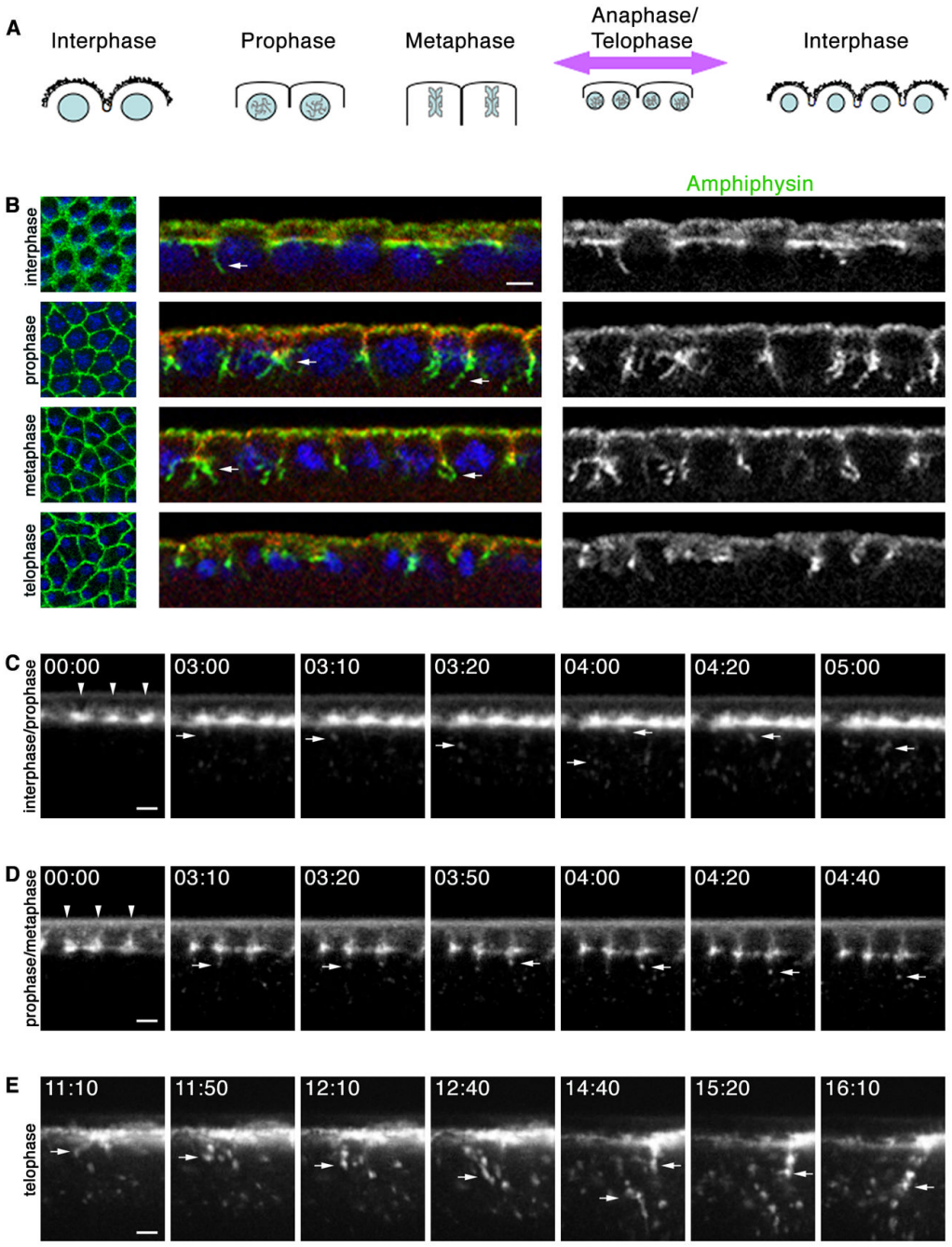

Figure 1.

Cell-cycle progression regulates endocytosis at early mitotic cycles. (A) Furrow dynamics at mitotic cycles (DNA, blue; somatic buds, jagged black lines). Cortex is maximally displaced when metaphase furrows regress (purple arrow). (B) Cross-sections at early mitotic cycle show few Amph (green) tubules (arrows) extend from somatic bud margins (Septin; red) at interphase, many tubules extend from metaphase furrow tips at prophase-metaphase, and no tubules extend from regressing metaphase furrows at telophase. DNA (blue) shows phase of cell cycle. (C–E) Time-lapse cross-sections after peri-vitelline injection of Alexa488-WGA. 00:00 time point set relative to start image acquisition (min:sec). (C) When injected at interphase, Alexa-488-WGA concentrates at somatic bud margins (arrowheads). As embryo

enters prophase, vesicles are released from margins (arrows). (D) When injected at interphase/prophase transition, Alexa488-WGA labels ingressing furrows (arrowheads). Vesicles (arrows) are released from furrow tips. (E) When injected at interphase, Alexa488-WGA patches blur as mitosis progresses. First frame shows onset of cortical displacement (large arrow) at late anaphase/telophase when metaphase furrows regress and dramatic endocytosis ensues (small arrows). See Movies S2, S3, S4. Bars are 5 μm.

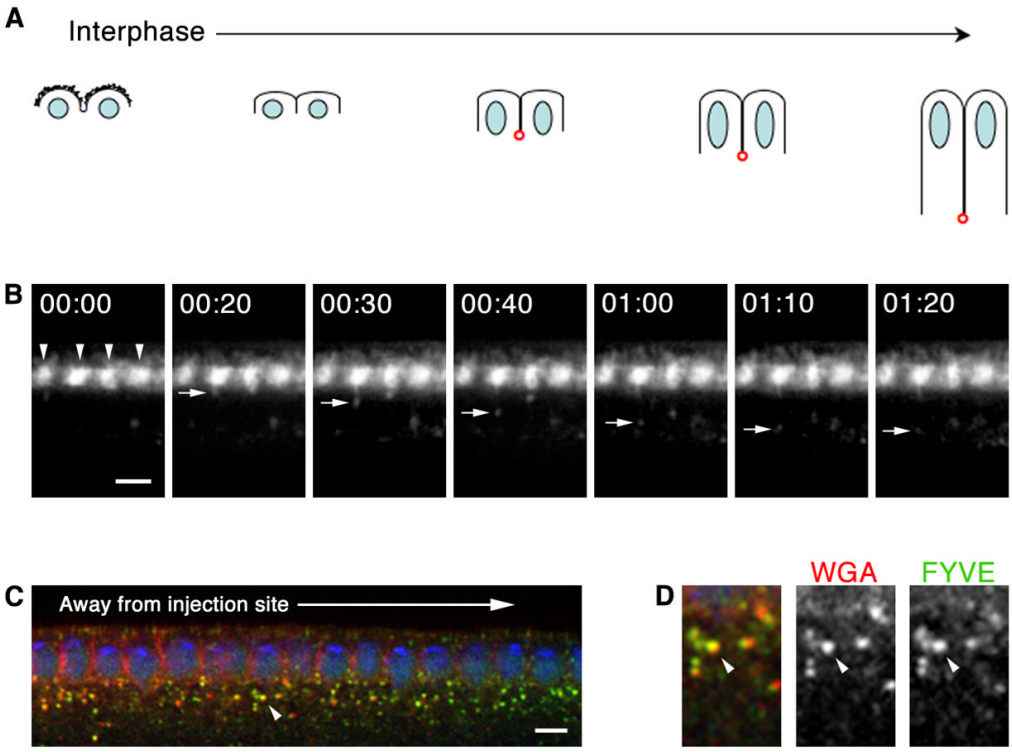

Figure 2.

Local endocytosis occurs at forming cellularization furrows. (A) Furrow dynamics at cellularization (DNA, blue; somatic buds, jagged black lines; furrow canals, red). (B–D) Cross-sections after peri-vitelline injection of Alexa488-WGA. (B) Time-lapse shows Alexa488-WGA concentrates at somatic bud margins (arrowheads). Vesicles bud as cellularization furrows form. 00:00 time point set relative to vesicle budding (min:sec). See Movie S2. (C) Peri-vitelline injection of Alexa546-WGA (red), followed by 15 minute chase and fixation. Embryo expresses FYVE-GFP (green). WGA binds embryo surface immediate to injection site. WGA label lengthens basally between nuclei (DNA; blue) as furrows ingress. WGA vesicles incorporate into early endosomes (arrowhead). (D) Higher magnification view of early endosome indicated in B by arrowhead shows Alexa546-WGA (red) and FYVE-GFP (green) co-localize. Bars are 5 μm.

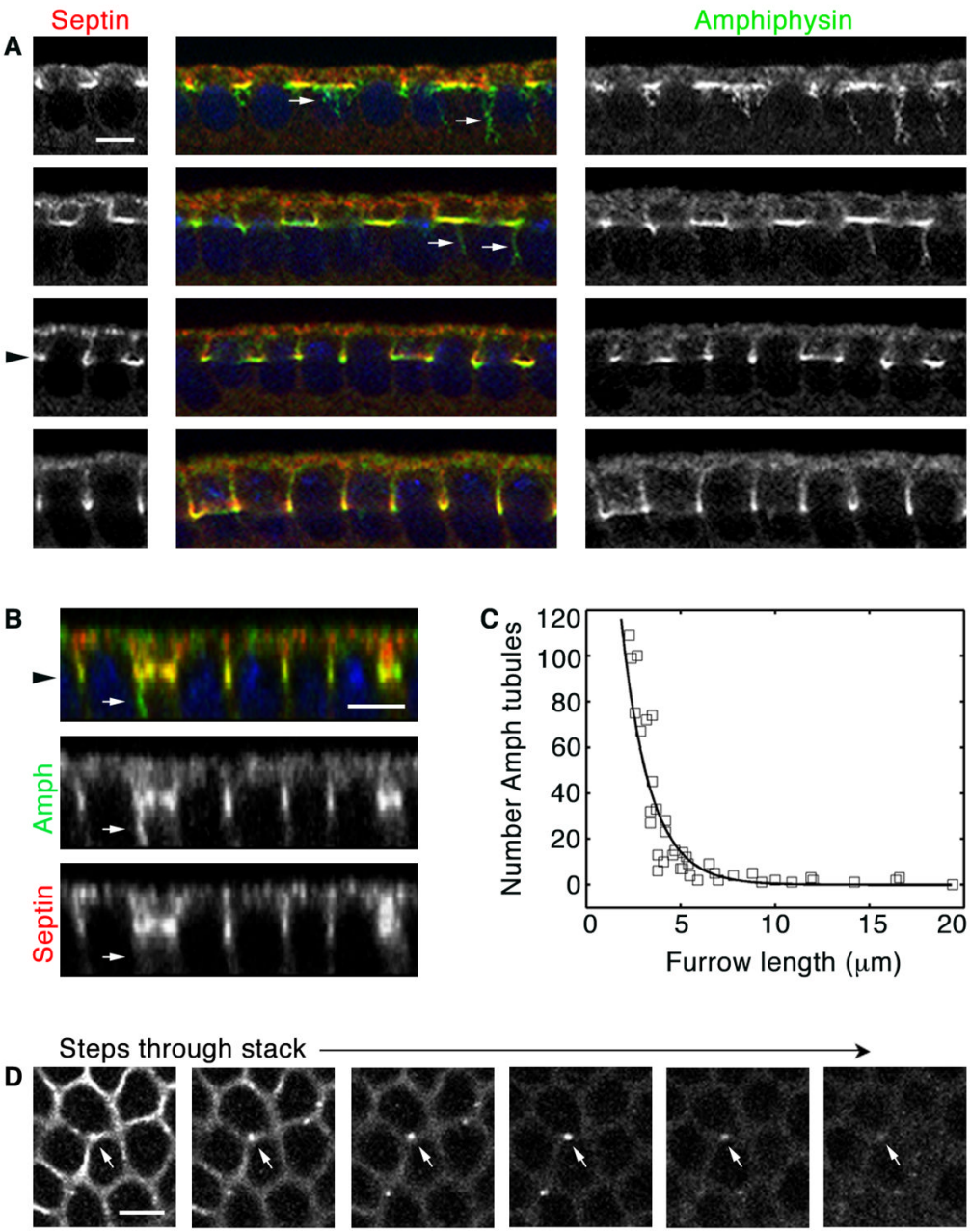

Figure 3.

Local endocytosis is regulated at cellularization. (A) Cross-sections show many Amph (green) tubules (arrows) extend from incipient furrow tips (Septin; red). At 5 μm furrow length furrow canals are assembled (level of black arrowhead), and few tubules are seen. (B) Projected Z-section shows Amph (green) tubule (arrows) extending from furrow tip (septin; red; level of black arrowhead). (C) Number Amph tubules in wild-type embryos during cellularization. Each point represents one embryo with 160–180 furrows analyzed. Tubules are not detected at ≥ 5 μm furrow length. (D) Sequential planes in a Z-stack (moving deeper from left to right, 0. 5 μm step) show an Amph structure in cross-section (arrow). It appears as a circle, consistent with it being a tubule. Bars are 5 μm.

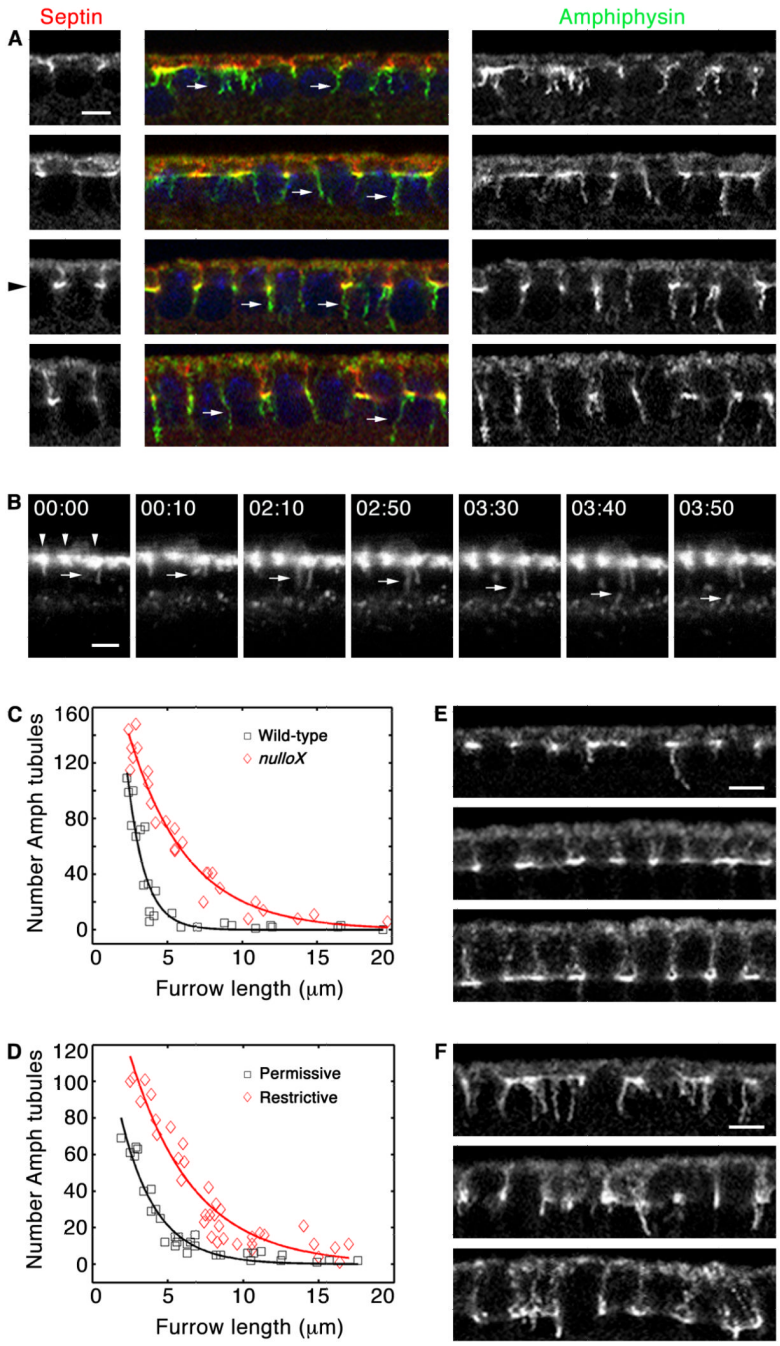

Figure 4.

Nullo regulates endocytosis at cellularization. (A) Cross-sections of *nulloX* embryos show many Amph (green) tubules (arrows) extend from incipient furrow tips (Septin; red). At 5 μm furrow length (level of black arrowhead), Amph tubules persist. (B) Time-lapse cross-sections of *nulloX* embryo after peri-vitelline injection of Alexa488-WGA. Alexa488-WGA concentrates at somatic bud margins (arrowheads). Budding vesicles distend into membrane tubules (arrows), persisting up to several minutes before release. 00:00 time point set relative to vesicle budding (min:sec). See Movie S3. (C) Number Amph tubules in wild-type (black) versus *nulloX* (red) embryos during cellularization. Each point represents one embryo with 160–180 furrows analyzed. Tubules persist at ≥ 5 μm furrow length in *nulloX*.

(D) Number Amph tubules at permissive (black) versus restrictive (red) temperatures in *shi*^{ts1} embryos during cellularization, quantified as in C. Tubules persist at ≥ 5 μm furrow length at restrictive temperature. (E, F) Cross-sections show Amph tubules in *shi*^{ts1} embryos. (E) At permissive temperature, few tubules are seen at ≥ 5 μm furrow length. (F) At restrictive temperature, tubules persist at ≥ 5 μm furrow length. Bars are5 μm.

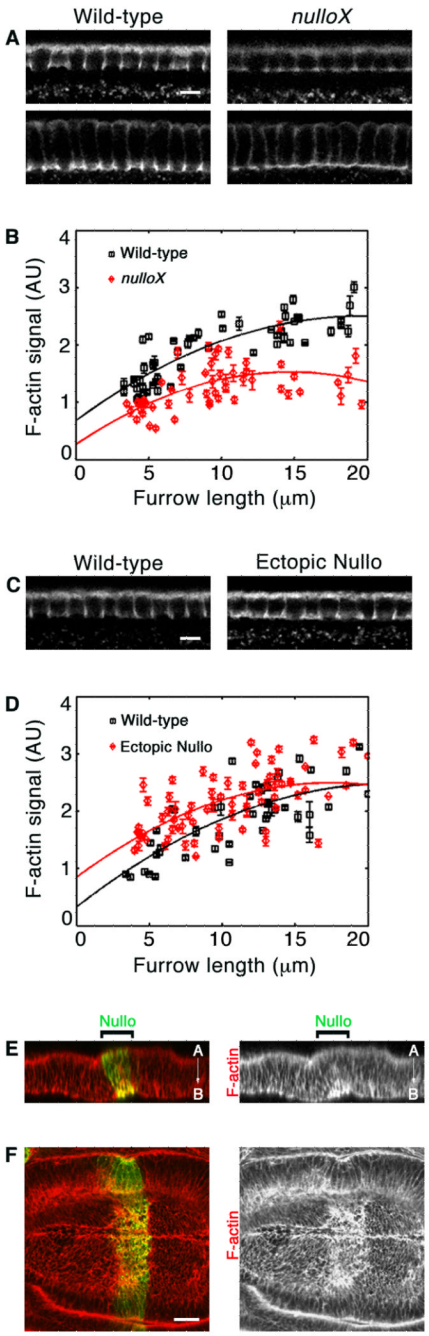

Figure 5.

Nullo regulates cortical F-actin. (A, C) Cross-sections of F-actin in comparably staged cellularizing embryos. Images collected at same settings for wild-type versus *nullo* manipulation. (A) *nulloX* furrow canals show reduced F-actin. (B) F-actin in wild-type (black) versus *nullo*X (red) furrow canals, measured by intensity of phalloidin staining. Each point represents one embryo with 75–100 furrow canals analyzed. Error bars show standard deviation. (C) Ectopic Nullo furrow canals show increased actin. (D) F-actin in wild-type (black) versus ectopic Nullo (red) furrow canals, quantified as in B. (E–F) F-actin (red) in an imaginal wing disc expressing a stripe of ectopic Nullo (green). (E) Projected Z-section shows that F-actin is increased at basal-lateral cortex of Nullo-expressing cells (A, apical; B,

basal). (F) *En face* image from a single basal plane of the disc showing a stripe of F-actin increase in Nullo-expressing cells. Bars are 5 μm in A and C, and 20 μm in F.

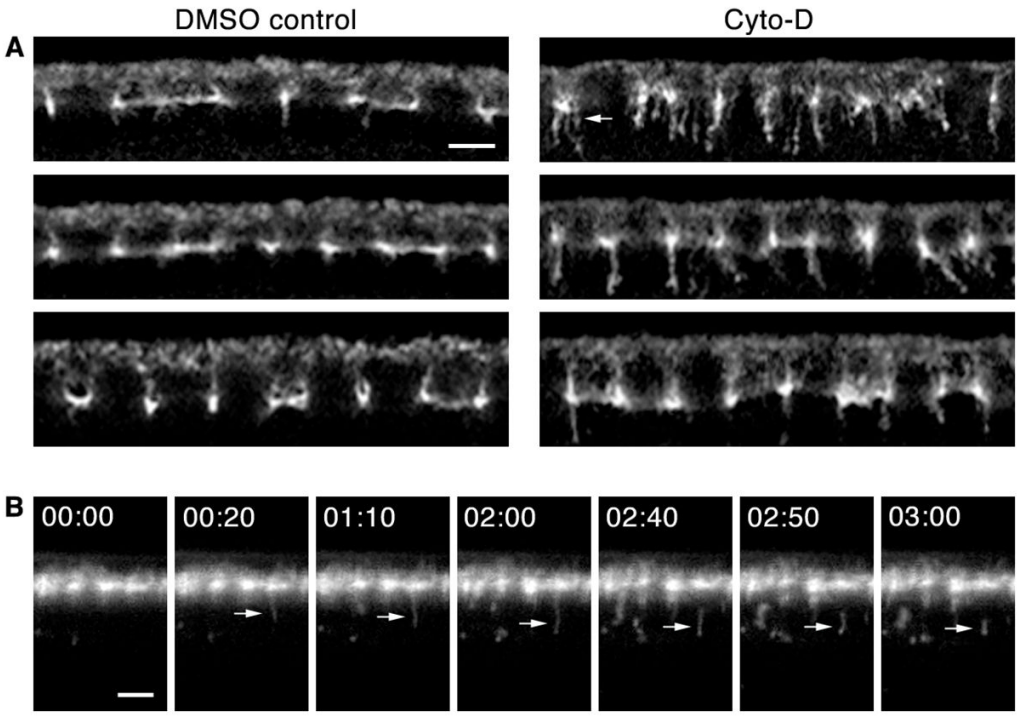

Figure 6.

F-actin disruption impairs endocytic scission at cellularization. (A) Cross-sections of Cyto-D versus DMSO control embryos. Amph tubules increase in number after Cyto-D treatment. At earliest cellularization multiple tubules extend from furrow tips (arrow). (B) Time-lapse cross-sections after co-peri-vitelline injection of Alexa488-WGA and Cyto-D. Some budding vesicles distend into tubules (arrow) that persist several minutes before release. 00:00 time point set relative to vesicle budding (min:sec). See Movie S4. Bars are 5 μm.

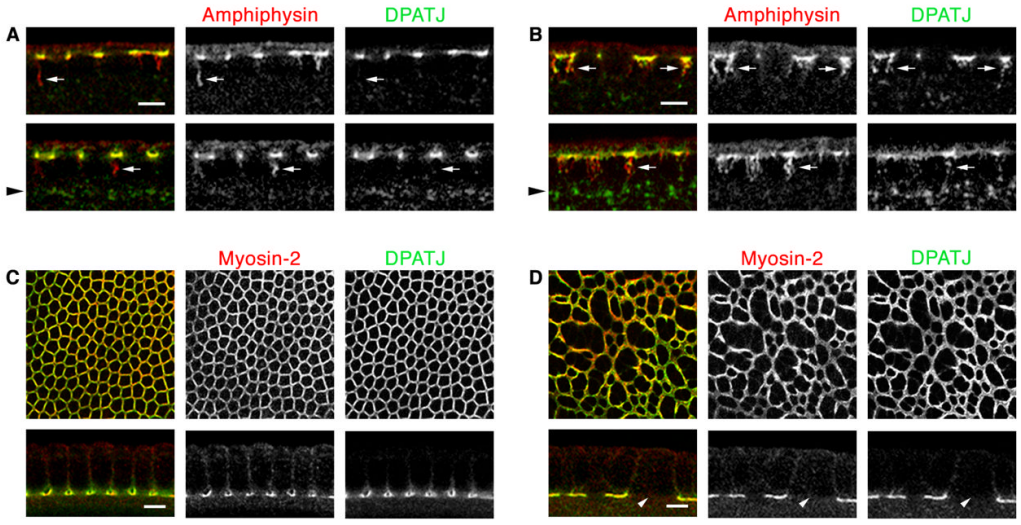

Figure 7.

Persistent Amph tubules deplete furrow canal components at cellularization. (A, B) Cross-sections show DPATJ (green) and Amph (red) tubules. Arrowheads indicate region of early endosomes. (A) DPATJ accumulates in wild-type furrow canals, but is rarely seen in Amph tubules (arrows). Some DPATJ is at early endosomes. (B) DPATJ (green) accumulates in *nulloX* furrow canals, but also enters Amph tubules (arrows). Increased levels DPATJ are at *nulloX* early endosomes. (C, D) En face images of furrow canals and cross-sections show DPATJ (green) and Myosin-2 (red). (C) DPATJ accumulates with Myosin-2 in wild-type furrow canals. (D) DPATJ and Myosin-2 are depleted from some *nulloX* furrow canals (arrow). Bars are 5 μm.